A WIND MODEL FOR AN ELEVATED STOL-PORT CONFIGURATION

by

J. A. Peterka*
and
J. E. Cermak**

October 1973

Prepared under Contract No. NAS2-7396 by
Fluid Mechanics Program
Fluid Dynamics and Diffusion Laboratory
Department of Civil Engineering
Colorado State University
Fort Collins, Colorado

for

AMES RESEARCH CENTER

NATIONAL AERONAUTICS AND SPACE ADMINISTRATION

Moffett Field, California 94035

---

*Assistant Professor
**Professor-in-Charge, Fluid Mechanics Program

CER73-74JAP-JEC10

ABSTRACT

Measurements of mean velocity magnitude and direction as well as three-dimensional turbulence intensity were made in the flow over a model of an elevated STOL-port. A 1:300 scale model was placed in a wind tunnel flow simulating the mean velocity profile and turbulence characteristics of atmospheric winds over a typical city environment excluding detailed wake structures of possible nearby buildings. Hot-wire anemometer measurements of velocity and turbulence were made along approach and departure paths of aircraft operating on the runway centerline and at specified lateral distances from the centerline. Approach flow directions simulated were 0 and 30 degrees to the runway centerline.

ACKNOWLEDGMENTS

The support of NASA, Ames Research Center in carrying out this study is gratefully acknowledged. Fabrication of the structure model was accomplished by personnel of the Engineering Research Center Machine Shop. Mr. Craig Hansen was responsible for instrumentation checkout and data acquisition. Assistance in obtaining data was provided by Mr. Tom Hoot and Mr. Gordon Scott.

TABLE OF CONTENTS

LIST OF TABLES

LIST OF FIGURES

LIST OF SYMBOLS

Symbol	Definition
X	coordinate axis parallel to STOL port centerline, positive upwind, zero at downwind edge of structure
Y	horizontal coordinate with zero on center data plane
Z	vertical coordinate, positive downward, zero on the top surface of the STOL port
U	mean velocity in X direction
V	mean velocity in Y direction
W	mean velocity in Z direction
U_{vector}	mean velocity vector magnitude
U_{∞}	value of U_{vector} above the boundary layer
u	fluctuating velocity in X direction
v	fluctuating velocity in Y direction
w	fluctuating velocity in Z direction
U_T	flow calibrator velocity
α	horizontal angle of U_{vector} in X, Y, Z coordinate system
β	vertical angle of U_{vector} in X, Y, Z coordinate system
θ	flow calibrator angle of incidence
A,B,C $\alpha_1,\alpha_2,\alpha_3$	calibration constants
E	mean voltage

1. INTRODUCTION

With the serious consideration of STOL aircraft as a major transportation mode, extensive investigations of STOL feasibility have been and are underway. One of the important factors in STOL-port design recognized by the FAA [1] is the effect of winds on aircraft operating from these facilities. Interest in this problem has accelerated in the last few years as evidenced by an increased level of investigation. Several investigators have discussed the effects of atmospheric turbulence on small aircraft performance [2, 3, 4]. Cass et al. [5] investigated the characteristics of turbulence about an airport site and found agreement on the influence of nearby buildings with a study by Colmer [6] of the wake structure behind an isolated hanger. Additional field measurements of turbulence in aircraft landing patterns near the Rock of Gibralter by Burnham and Spavins [7] showed intense turbulence for certain wind directions. Kurkowski et al. [8] have presented an improved turbulence model for use in flight simulations.

One STOL-port configuration under study is an elevated structure. It would have the advantage of getting an aircraft up away rapidly from turbulence associated with surrounding structures. One potential problem for this type of STOL-port is the influence of the structure itself on the winds in the regions through which the aircraft must fly. A preliminary, qualitative evaluation of STOL-port design was performed by Parker et al. [9] which showed that proper design could substantially alleviate structure induced flow problems. The purpose of the present study was to determine quantitatively the influence of a proposed

elevated STOL-port on the mean flow and turbulence over the structure. The results of this study are to be incorporated into a piloted-simulator to determine the effect on pilot-vehicle performance.

The study was performed by placing a model of the proposed elevated STOL-port in a wind tunnel specifically designed to simulate atmospheric winds. Proper modeling of the atmospheric boundary layer flow approaching the model is essential in providing accurate determination of the flow characteristics. Modeling criteria are discussed in Refs. 10 and 11. Mean velocity and three-dimensional turbulence measurements were made along typical approach and departure paths for STOL aircraft. Two wind directions were employed: one parallel to the flight path and one 30 degrees to the flight path. Measurements without the model in place allowed the influence of the structure to be evaluated.

2. EXPERIMENTAL CONFIGURATION

2.1 Wind Tunnel

The wind study was performed in the Environmental Wind Tunnel located in the Fluid Dynamics and Diffusion Laboratory at Colorado State University, Fig. 1. The tunnel is an open circuit facility driven by a variable pitch propeller. The test section is nominally 12 ft (3.66 m) wide, 8 ft (2.44 m) high, and 52 ft (15.8 m) long. The roof is adjustable to maintain a zero pressure gradient along the test section. The mean velocity can be adjusted continuously from 2 to 24 fps (0.61 to 7.31 mps) with the 10 hp motor and to a maximum velocity of 60 fps (18.3 mps) with the 150 hp motor.

2.2 Model

The elevated STOL-port structure has dimensions of 2200 ft (670.5 m) by 1200 ft (365.8 m) by 100 ft (30.5 m) high. In order to provide maximum resolution in the data, the largest scale model feasible within the physical limitations imposed by the wind tunnel was chosen. Scale selected was 1:300. Dimensions of the scaled model were 88 in (2.23 m) long, 48 in (1.22 m) wide, and 4 in (10.2 cm) high. The model was placed 25 ft (7.6 m) from the test section entrance on a turntable to allow ease of rotation. The turbulent boundary layer approaching the structure was developed with a carefully designed trip at the test section entrance 12 in (30.5 cm) high consisting of 2.5 in (6.4 cm) diameter tubes followed by ½ in (1.27 cm) gravel uniformly spread over the floor. A photograph of the model in-place in the wind tunnel is shown in Fig. 2.

No attempt was made to simulate the detailed wake of individual structures in the flow approaching the model. Instead, a turbulent boundary layer was generated whose characteristics simulated a typical atmospheric boundary-layer flow over an urban environment.

3. INSTRUMENTATION AND DATA ACQUISITION

3.1 Flow Visualization

Visualization of the flow over the model is helpful in understanding and interpreting mean and fluctuating pressures, in defining zones of separated and reattached flow, and in identifying size and intensity of vortices generated by building corners. Titanium tetrachloride smoke was released from sources on and near the model and photographic records were made of the flow. Conclusions based on these observations are discussed in section 4.1.

3.2 Mean Velocity and Flow Direction

To measure three components of mean flow and the mean velocity direction a new hot-wire anemometer measurement scheme which has been under development at the Fluid Dynamics and Diffusion Laboratory at Colorado State University was employed. The procedure utilized a conventional 45 degree yawed hot-wire sensing element 0.00015 in. (0.0038 mm) in diameter with an active length of 0.050 in. (1.25 mm). A Colorado State University hot-wire anemometer unit was used with the sensing element. The unit is characterized by good stability and high signal to noise ratio. A photograph of the probe is shown in Fig. 3.

Operation of the measurement system required that the hot-wire be calibrated for flow speed and angle-of-flow incidence to the wire. A Thermo-Systems flow calibrator was used with a Colorado State University built probe positioner. The calibration data was fit to a modified King's law equation of the form

$$E^2 = A + BU_T^C f(\theta)$$

$$f(\theta) = 1 + \alpha_1\theta + \alpha_2\theta^2 + \alpha_3\theta^3 \quad (1)$$

where U_T and θ are the velocity and angle to the wire (0 degrees was parallel to the wire) of the calibration flow, E is the mean voltage output from the anemometer, and A, B, C, α_1, α_2, α_3 are calibration constants used to fit the equation to the data. Thirty calibration points representing 5 velocities at 6 angles were used in a computer program to fit the calibration-equation coefficients by least squares. Calculations were performed on the Colorado State University CDC6400 computer. A typical calibration is shown in Fig. 4.

To obtain mean velocity data, the probe was mounted in the wind tunnel approximately 20 degrees to the horizontal plane and 20 degrees to the tunnel vertical centerline plane. Twelve to 15 mean voltages at different rotational positions were obtained using an integrating digital voltmeter for 30 seconds. This positioned the sensing element at angles to the mean flow ranging from about 20° to 70°. Data was reduced by finding the three mean velocity components U_m, V_m, W_m which provided the least squares fit of the data to Eq. 1 in a coordinate system aligned with the probe axis of rotation. Because the equation cannot be solved explicitly for the velocity components, an iteration method was devised to converge to the correct solution from initial velocity estimates. Convergence was obtained in 6 to 8 interations with simple initial estimates. A vector rotation was applied to the velocity components to transform them from the probe oriented coordinate system into the coordinate system defined for the STOL-port (Section 3.4 and Figure 5).

Horizontal and vertical flow angles were computed from the velocity components. All calculations were performed on the Colorado State University CDC6400 computer.

The probe attitude relative to the wind tunnel coordinate system was set with an optical alignment system. A laser light source was aligned along the data plane being measured. A mirror mounted to the probe support reflected the light back to a target placed near the laser. Using this system, the probe could be aligned to a predetermined attitude within 0.2 degrees.

The accuracy of the mean velocity measurements was measured in such a way that the error included both the variablity inherent in the wind-tunnel flow and the uncertainty due to the measurement probe itself. The analysis was performed by measuring several vertical profiles in the wind tunnel with the model removed but the roughness remaining. The total error was the difference between the assumed zero angle of flow and the angle measured with the probe. The standard deviation in α (the flow angle in the horizontal plane) was 0.90 degrees while the standard deviation in β (the flow angle in the vertical plane) was 0.79 degrees. These figures compare favorably to the angular resolution of 5.0 degrees in the horizontal and 1.0 degrees in the vertical requested in the statement of work defining the scope of this investigation. The error in the magnitude of the total velocity vector was not measured precisely because the errors in the comparative pitot tube measurements appeared from tests to be larger than those of the probe itself. The error appeared to be one percent or less.

3.3 Turbulence Intensities

Measurement of turbulence intensity was made with a standard X-wire probe. The probe was aligned to the mean flow direction determined previously with the optical alignment system described above. Each of the wires was calibrated individually with the Thermo-Systems calibrator. Data reduction used the procedure described by Klatt [12] which accounts for differences in wire calibration for each wire. The turbulence quantities calculated were u_{rms}/U_{vector}, v_{rms}/U_{vector}, and w_{rms}/U_{vector} where u, v, and w are the three fluctuating velocities in directions X, Y, Z and U_{vector} is the local mean velocity magnitude.

An independent check of the crossed-wire turbulence results was made by measuring at several data locations the longitudinal component of velocity fluctuation with a hot-wire placed normal to the flow. The results of the comparative measurements are shown by the triangles and squares in Fig. 5. The results are in excellent agreement.

3.4 Data Locations

Except for vertical profiles to determine the characteristics of the approach flow, all data was taken along data lines lying within data planes. Two data planes were used: 1) Center Data Plane, a vertical plane through the center of the building 600 ft (182.0 m) from either side and 2) Side Data Plane, a plane parallel to the Center Plane but 150 ft (45.7 m) in from one side. These data planes provided information on the conditions an aircraft could experience during take-off or landing at the center of the runway and near the edge of the structure.

A data line was established in each data plane along lines expected to be used for approach, runway, and departure. The approach

segment was defined as a line extending upward at a 7.5 degree angle to the horizontal in a downwind direction from a point on the runway centerline 350 ft (106.7 m) from the downwind edge of the roof. The departure segment was defined as a line extending upwards at a 7.5 degree angle to the horizontal in an upwind direction from a point on the runway centerline 1000 ft (304.8 m) from the downwind edge of the roof. The runway segment was defined as a line 15 ft (4.6 m) above the runway centerline that connected the approach segment to the departure segment. The data lines are shown in Fig. 6.

Data points were located along the data lines to provide adequate resolution of the measurements. Five data points were evenly spaced along the runway segment, seven points were located along the approach segment and thirteen points were located along the departure segment for a total of twenty-five data points per data line.

A coordinate system fixed to the STOL-port was defined for data reporting purposes (Fig. 6). Y = 0 defined the particular data plane of interest. Negative Z represented height above the STOL-port roof while positive X was distance into the wind from the downwind edge of the roof. This coordinate system is the same as provided in the statement of work defining the scope of this investigation.

4. RESULTS

4.1 Flow Visualization

Structures with sharp corners placed in an atmospheric flow are known to generate vortices from leading corners when the wind is at an angle to a building side. Increased turbulence in the approach flow tends to break down organized vortex structures more rapidly. A primary objective of the visualization was to identfy this vortex structure by observing its strength and coherence downstream. Smoke flow showed significant vorticity with an axis parallel to the structure's long side over the model near the windward side for flow approaching at 30 degrees to the building long axis. This vorticity emanated from the leading corner but was fed along its length by separation of flow along the leading edge of the roof. Flow reattached to the roof not far downstream from the leading edge, but neither the separation streamline nor reattachment region were well defined. Diffusion of smoke occurred so rapidly in the turbulence that the above described phenomena could not be adequately captured on film. The influence of this vorticity on flight patterns should be confined to the windward side data plane for the 30 degree wind.

Lifting of the flow approaching the structure appeared to extend to rather high elevations over the building. A variation in vertical flow angle of possible significance to aircraft was observed with the smoke for all cases in the region over the structure's leading edge. All conclusions obtained from flow visualization were confirmed with the velocity measurements reported in sections 4.3 and 4.4.

4.2 Data Scaling

Velocity data was taken for a reference velocity outside the boundary layer of 23.2 fps (7.07 mps). This provided a wind tunnel

Reynolds number ($\frac{UD}{\nu}$) based on building height and approach velocity at that height of 3×10^4. This is the smallest of the Reynolds numbers which can be calculated using building geometry for the length scale, and a characteristic approach velocity. At this value of Reynolds number, the flow structure should be Reynolds number independent; that is a component of mean velocity at any point in the flow normalized by the velocity U_∞ at the edge of the boundary layer should be independent of the approach velocity U_∞. In addition, a turbulence intensity as defined in section 3.3 at any point in the flow should be independent of U_∞. Thus the data taken at 23.2 fps (7.07 mps) can be used to obtain mean and root-mean-square velocities for any desired approach velocity. Mean velocity magnitudes are obtained by simply multiplying the nondimensional velocities (i.e. U/U_∞) by the desired free stream velocity. Root-mean-square velocities must, in addition, be mutiplied by the nondimensionalized local mean velocity, $\frac{U_{vector}}{U_\infty}$, since the turbulence quantities were made nondimensional with the local velocity according to standard practice.

An experimental verification of the Reynolds number independence was performed by remeasuring several quantities at a different approach velocity. A comparison of mean velocity profiles taken along the upwind centerline data line for a 30 degree approach wind for 23.2 fps (7.07 mps) and 15 fps (4.57 mps) is shown in Fig. 7. The comparison is good. The profile shown should be valid for all approach velocities above 15 fps. A comparison of longitudinal turbulence intensity for a portion of the same data line for identical velocities is shown by the circles and triangles in Fig. 5. The agreement is within the accuracy required for the study. The turbulent intensities are thus valid for the same range of approach velocities as the mean velocity.

4.3 Mean Velocities

Mean velocity profiles were obtained at the model site with the building removed to provide a baseline for comparison of data with the model in place. These profiles are shown in Figs. 8 and 9. The vertical coordinate shown, $-\frac{(Z-H)}{\delta}$, is in the coordinate system defined in Section 3.4 and represents the nondimensional distance above the ground level. The velocities are shown in both logarithmic and semi-logarithmic form to demonstrate the characteristics of the boundary layer. For the logarithmic description, the velocity profile is expressed in the following form:

$$\frac{U}{U_\infty} = \left(-\frac{Z-H}{\delta}\right)^{0.345}$$

The exponent 0.345 is centered within the range of values expected for a city environment. The velocity profile in semi-logarithmic form shows a linear profile as is expected for a neutrally stable atmospheric boundary layer. The roughness length Z_o is 7.2 ft. (2.2 m) in the full scale, a very reasonable value for a city roughness.

Mean velocity magnitudes and directions with the model in place are recorded in Tables 1 and 2. Table 1 shows the magnitude of the mean velocity vector and its horizontal and vertical angles to the reference coordinate system for each data point in the 5 data planes of interest. The velocity vector magnitude is recorded as U_{vector}/U_∞ where U_∞ is the velocity at the edge of the boundary layer. Definitions of the horizontal angle α and vertical angle β are given in Fig. 10. With the model oriented so that the wind vector is from an angle to the left for a landing or departing aircraft, an α more positive than the prevailing wind angle would indicate a local wind to the right of the

prevailing direction. A positive β angle indicates an upward vertical component in the wind vector. The data planes investigated were the center and one side plane for a zero degree approach wind and the center and both side planes for a 30 degree wind approaching from the left. Table 1 also shows the magnitude of the mean velocity vector on the center data plane at zero degree wind azimuth with the STOL port removed from the wind tunnel. The α and β angles were nominally zero for that case.

A breakdown for the velocity vector into components is shown in Table 2. Data is supplied only for the 30 degree case since the V and W components were negligibly small for the 0 degree cases.

An overall view of the mean flow characteristics along the data lines is shown in Fig. 11. The individual arrows represent the magnitude and horizontal direction of the mean flow measured at the arrow base on three data lines. The strongest effects are seen in the upwind side data plane. The effect of the model on the velocity magnitude can be seen in Fig. 12. The three curves represent (1) the approach flow without the model and (2) with the model, the velocities on the approach and departure segments of the center data line for a zero degree wind. Reduction in wind velocity with the model in place is evident for both cases.

Of great concern to aircraft is the angle of the flow over the structure -- in particular, rapid changes in vertical angle of flow may cause difficulties for small aircraft. Plots of vertical and horizontal angles for the mean flow vector are plotted in Figs. 13 through 16. Figure 13 shows the vertical angle for the data lines in the center and side planes for a zero degree wind. Extremum in angle

occur at or just off the edge of the structure with little change in angle over the center portion of the structure. Figure 14 shows the horizontal flow angle for the same conditions as the previous figure. No sharp gradients exist in the angles. The approximately one degree bias in the center plane data is due to a small cross flow tendency in the lower third of the 8 ft (2.44 m) height of the wind tunnel flow (the model was aligned precisely with the geometrical wind tunnel axis).

The vertical flow angle for the center plane and both side planes is shown in Fig. 15. All three show the same qualitative features with the magnitude of effect differing slightly. Again, the largest gradient in angle occurred near the edges of the model. Figure 16 shows the horizontal angle for the same conditions. The gradient of angle is severe only for the windward side plane, an effect also noted in Fig. 11. Smoke flow observations tended to show the same effect.

4.4 Turbulence Intensities

Longitudinal turbulence intensity at the building site without the model in place is shown in Fig. 17 as a function of height above the surface. The data provides a comparison for data taken with the model in place.

Turbulence intensities in the three directions defined by the coordinate system defined in Section 3.4 are listed in Table 3. Measurement positions for two data planes at a 0 degree wind and three data planes at 30 degree wind were the same as for mean velocities. Some characteristics of the turbulent field can be seen from Figs. 18 and 19. For a 0 degree wind, the longitudinal fluctuations varied

smoothly reaching a maximum amplitude of 15 to 17 percent in the two data planes at about 80 to 100 ft above the STOL port surface on the departure line. The fluctuations varied more for the 30 degree wind (Fig. 19) reaching a maximum value of 23 percent near the takeoff point on the departure line on the windward data plane. Maximum value on the other two planes at 30° were 12 percent. The spatial variability of the windward data was confirmed with repeat measurements. The turbulence components in the Y and Z directions generally followed the same trends as the longitudinal component, but at lower amplitudes.

5. CONCLUSIONS

Measurements of mean velocity magnitude and direction as well as three-dimensional turbulence intensity were made in the flow over a modeled STOL port. The flow approaching the model was representative of flow over a city environment excluding detailed wake structures of possible nearby buildings. The measurements were made along approach and departure paths of aircraft operating on the building center line and 150 ft in from each side of the structure with wind directions parallel and 30 degrees to the flight path. Results of the measurements showed the worst environment of those studied to be the flight path nearest the windward side of the STOL-port with a 30 degree wind. Sizable turbulence intensities and gradients of mean flow angle were found, however, even for the centerline with a 0 degree wind.

The present study did not attempt to modify the flow characteristics over the structure with vortex spoiling devices. Relatively simple modifications to the local geometry at the building edge which would not interfere with aircraft safety should help to alleviate some of the adverse flow characteristics seen in this study. Since the elevated STOL port was conceived for use near a large city, the wakes of other structures in the vicinity may cause larger effects on the flow than the structure itself. For this reason, additional wind-tunnel tests with realistic city surroundings should be undertaken before suitability of the elevated STOL port concept is accepted.

REFERENCES

1. Planning and Design Criteria for Metropolitan STOL Ports, Federal Aviation Administration, Washington, D.C., Nov. 1970.

2. Burnham, J., "A Note on Turbulence Problems Associated with Take-Off and Landing," TR67240, Royal Aircraft Establishment, Farnborough Hants, England, Sept. 1967.

3. Burnham, J. and F. O'Hara, "The Atmospheric Environment and Aircraft - Now and the Future," TM AERO 1067, Royal Aircraft Establishment, Farnborough Hants, England, July 1968.

4. Morrissey, E. G., "An Approximate Method for Calculating Critical Gust Statistics for STOL Operations," Canadian Meterological Research Report, Department of Transport, Toronto, Canada, April 1970.

5. Cass, Stanley D., J. R. Scoggins, and H. L. Chevalier, "Low-Altitude Atmospheric Turbulence around an Airport," Jl. Aircraft, Vol. 10, pp. 157-163, March 1973.

6. Colmer, M., "Some Full-Scale Measurements of the Flow in the Wake of a Hangar," Aeronautical Research Council Current Papers No. 1166, Ministry of Aviation Supply, Her Majesty's Stationery Office, London, England, 1971.

7. Burnham, J. and C. S. Spavins, "Gusts on the Approach at Gibralter Airfield," TR 65099, Royal Aircraft Establishment, Farnborough Hants, England, May 1965.

8. Kurkowski, R. L., G. H. Fichtl, and J. Gera, "Development of Turbulence and Wind Shear Models for Simulator Application," NASA Aircraft Safety and Operating Problems, Vol. 1, NASA Langley Research Center, Hampton, Virginia, pp. 291-306, May 1971.

9. Parker, H. M., J. N. Blanton, and K. J. Grunwald, "Some Aspects of the Aerodynamics of STOL Ports," NASA Aircraft Safety and Operating Problems, Vol. 1, NASA Langley Research Center, Hampton, Virginia, pp. 263-276, May 1971.

10. Cermak, J. E., "Laboratory Simulation of the Atmospheric Boundary Layer," AIAA Jl., Vol. 9, pp. 1746-1754, Sept. 1971.

11. Cermak, J. E., "Air Motion in and Near Cities - Determination by Laboratory Simulation," Tech. Paper CEO70-71JEC27, Fluid Dynamics and Diffusion Laboratory, Colorado State University, Fort Collins, Colorado, July 1970.

12. Klatt, F., "The X Hot-Wire Probe in a Plane Flow Field," DISA Information, No. 8, DISA Elektronik, Herler, Denmark, July 1969.

TABLE 1

NORMALIZED MEAN VELOCITIES AND ANGLES
(U_∞ = 23.2 ft/sec)

		WITHOUT MODEL	WIND AT 0 DEGREES CENTER DATA PLANE			WIND AT 0 DEGREES SIDE DATA PLANE			WIND AT 30 DEGREES LEE SIDE DATA PLANE			WIND AT 30 DEGREES CENTER DATA PLANE			WIND AT 30 DEGREES WINDWARD SIDE DATA PLANE		
X(ft)	-Z(ft)	$\frac{U_{vector}}{U_\infty}$	$\frac{U_{vector}}{U_\infty}$	α (Deg)	β (Deg)	U_{vector}	α (Deg)	β (Deg)	$\frac{U_{vector}}{U_\infty}$	α (Deg)	β (Deg)	$\frac{U_{vector}}{U_\infty}$	α (Deg)	β (Deg)	$\frac{U_{vector}}{U_\infty}$	α (Deg)	β (Deg)
-750	175	0.90	0.90	1.2	-2.5	0.85	.3	-2.2	0.78	-30.1	-3.0	0.79	-32.3	-3.7	0.76	-32.7	-1.4
-300	100	0.81	0.80	0.7	-2.3	0.77	-0.8	-3.5	0.75	-29.1	-2.6	0.74	-30.5	-3.7	0.73	-34.0	-0.1
-150	81	0.79	0.72	0.9	-1.8	0.76	0.9	-1.8	0.71	-29.5	-2.5	0.73	-29.2	-2.9	0.75	-34.0	0.6
- 50	68	0.77	0.71	0.9	- .8	0.73	-0.5	-1.8	0.70	-28.9	-1.4	0.69	-29.3	-1.7	0.68	-35.7	0.7
+ 50	54	0.74	0.67	0.7	- .1	0.69	-0.7	-0.2	0.68	-29.3	-0.3	0.64	-28.7	-1.1	0.63	-35.7	-0.2
150	41	0.71	0.64	1.3	.5	0.66	-0.6	0.6	0.67	-29.5	-0.3	0.59	-28.9	0.4	0.58	-30.1	1.6
250	28	0.69	0.60	1.1	1.6	0.60	-0.1	1.4	0.65	-29.9	0.0	0.56	-28.0	0.3	0.52	-29.9	0.9
350	15	0.65	0.56	1.5	1.4	0.56	-0.3	-0.2	0.61	-30.3	1.1	0.53	-27.1	0.4	0.49	-23.1	1.6
512	15	0.65	0.54	1.0	1.4	0.53	-0.6	1.0	0.63	-30.8	0.4	0.52	-28.5	0.5	0.47	-25.4	2.3
675	15	0.65	0.54	2.0	1.5	0.53	0.0	0.9	0.64	-32.2	0.0	0.52	-29.3	1.2	0.45	-25.8	1.8
838	15	0.65	0.52	1.3	1.5	0.53	0.2	1.3	0.62	-33.0	0.9	0.54	-28.8	1.1	0.44	-24.2	1.8
1000	15	0.65	0.51	1.9	1.3	0.53	-0.1	0.5	0.54	-34.3	1.1	0.57	-30.2	1.0	0.45	-25.9	2.0
1100	28	0.69	0.52	1.2	1.5	0.58	0.5	1.0	0.55	-33.9	1.5	0.62	-30.9	0.9	0.47	-30.6	1.3
1200	41	0.71	0.54	0.7	1.3	0.59	0.4	1.3	0.57	-34.0	0.8	0.66	-30.6	0.8	0.52	-35.1	1.3
1300	54	0.74	0.57	1.2	1.3	0.61	0.0	0.7				0.70	-31.4	0.5	0.57	-38.1	0.8
1400	68	0.77	0.62	0.7	1.3	0.62	0.5	2.4	0.63	-33.0	0.3	0.71	-31.5	0.6	0.60	-36.0	0.7
1500	81	0.79	0.64	1.0	1.2	0.68	0.3	0.5	0.64	-32.3	0.1	0.74	-30.8	0.8	0.63	-34.5	1.0
1600	94	0.81	0.70	0.4	.3	0.69	0.0	0.0	0.67	-31.5	0.2	0.73	-30.6	1.0	0.70	-33.6	0.0
1700	107	0.83	0.73	0.8	.7	0.75	1.0	0.0	0.71	-31.1	-0.5	0.70	-29.9	1.7	0.75	-33.5	0.3
1875	130	0.87	0.80	1.0	.7	0.80	1.7	0.5	0.77	-30.0	-0.1	0.70	-29.5	1.9	0.81	-30.6	0.4
2050	153	0.89	0.87	0.9	1.9	0.85	2.1	1.8	0.81	-28.8	2.0	0.82	-28.0	2.6	0.87	-29.2	0.6
2200	174	0.91	0.89	1.3	4.2	0.86	2.4	4.1	0.83	-29.5	3.8	0.85	-28.3	4.0	0.88	-28.7	1.6
2350	194	0.86	0.89	1.4	3.5	0.85	2.4	3.6	0.84	-29.6	2.8	0.87	-29.3	3.8	0.87	-28.9	1.5
2650	233	0.93	0.96	1.8	1.57	0.87	2.7	1.41	0.84	-27.9	1.5	0.86	-27.2	0.9	0.85	-28.5	2.3
2950	272	1.0	0.99	2.0	.43	0.91	2.7	.71	0.89	-27.3	-0.2	0.87	-27.4	0.8	0.90	-27.4	1.6

TABLE 2

MEAN VELOCITY COMPONENTS FOR 30 DEGREE WIND

		LEE SIDE DATA PLANE			CENTERLINE DATA PLANE			WINDWARD SIDE DATA PLANE		
X	-Z	$\frac{U}{U_\infty}$	$\frac{V}{U_\infty}$	$\frac{W}{U_\infty}$	$\frac{U}{U_\infty}$	$\frac{V}{U_\infty}$	$\frac{W}{U_\infty}$	$\frac{U}{U_\infty}$	$\frac{V}{U_\infty}$	$\frac{W}{U_\infty}$
-750	175	-.67	.39	.041	-.66	.41	.050	-.63	.41	.018
-300	100	-.65	.36	.033	-.64	.37	.048	-.61	.41	.0015
-150	81	-.62	.35	.031	-.63	.35	.037	-.62	.42	-.0074
- 50	68	-.61	.34	.017	-.60	.34	.020	-.55	.40	-.0084
50	54	-.59	.33	.0029	-.56	.31	.012	-.51	.37	.0020
150	41	-.58	.33	.0032	-.52	.29	-.0046	-.50	.29	-.016
250	28	-.57	.33	.0002	-.49	.26	-.0028	-.45	.26	-.0081
350	15	-.53	.31	-.012	-.47	.24	-.0036	-.45	.19	-.014
512	15	-.54	.32	-.0040	-.46	.25	-.0047	-.42	.20	-.019
675	15	-.54	.34	-.0007	-.45	.25	-.011	-.40	.20	-.014
838	15	-.52	.34	-.0098	-.47	.26	-.011	-.41	.18	-.014
1000	15	-.45	.31	-.011	-.49	.29	-.0095	-.40	.20	-.015
1100	28	-.45	.30	-.014	-.53	.32	-.010	-.41	.24	-.011
1200	41	-.47	.32	-.0075	-.57	.33	-.0093	-.42	.30	-.012
1300	54				-.60	.36	-.0064	-.45	.35	-.0077
1400	68	-.53	.34	-.0029	-.63	.38	-.0081	-.48	.35	-.0077
1500	81	-.54	.34	-.0014	-.64	.38	-.010	-.52	.36	-.011
1600	94	-.57	.35	-.0022	-.62	.37	-.013	-.56	.39	.0002
1700	107	-.61	.37	.0061	-.61	.35	-.021	-.63	.41	-.0043
1875	130	-.66	.38	.0013	-.61	.34	-.023	-.70	.41	-.0050
2050	153	-.70	.39	-.028	-.72	.38	-.037	-.76	.42	-.0094
2200	174	-.72	.41	-.055	-.75	.40	-.060	-.77	.42	-.024
2350	194	-.73	.41	-.042	-.75	.42	-.057	-.76	.42	-.022
2650	233	-.74	.40	-.022	-.77	.39	-.014	-.75	.41	-.035
2950	272	-.79	.41	.004	-.77	.40	-.012	-.80	.41	-.025

TABLE 3

THREE-DIMENSIONAL TURBULENCE INTENSITIES IN PERCENT

		WIND AT 0 DEGREES CENTERLINE DATA PLANE			WIND AT 0 DEGREES SIDE DATA PLANE			WIND AT 30 DEGREES LEE SIDE DATA PLANE			WIND AT 30 DEGREES CENTER DATA PLANE			WIND AT 30 DEGREES WINDWARD SIDE DATA PLANE		
X(ft)	-Z(ft)	$\frac{u_{rms}}{U_{vector}}$ (%)	$\frac{w_{rms}}{U_{vector}}$ (%)	$\frac{v_{rms}}{U_{vector}}$ (%)	$\frac{u_{rms}}{U_{vector}}$ (%)	$\frac{w_{rms}}{U_{vector}}$ (%)	$\frac{v_{rms}}{U_{vector}}$ (%)	$\frac{u_{rms}}{U_{vector}}$ (%)	$\frac{w_{rms}}{U_{vector}}$ (%)	$\frac{v_{rms}}{U_{vector}}$ (%)	$\frac{u_{rms}}{U_{vector}}$ (%)	$\frac{w_{rms}}{U_{vector}}$ (%)	$\frac{v_{rms}}{U_{vector}}$ (%)	$\frac{u_{rms}}{U_{vector}}$ (%)	$\frac{w_{rms}}{U_{vector}}$ (%)	$\frac{v_{rms}}{U_{vector}}$ (%)
-750	175	8.2	4.5	5.6	7.4	4.4	5.6	8.6	5.2	7.0	8.2	4.1	6.3	8.9	5.2	7.6
-300	100	10.7	5.7	7.1	9.8	5.1	7.0	9.5	5.6	7.4	9.5	5.2	8.2	9.9	5.7	8.2
-150	81	10.9	6.0	7.2	9.9	5.4	6.7	9.7	5.4	7.5	11.3	5.8	7.9	11.0	6.4	8.7
-50	68	11.0	6.0	7.2	9.8	5.3	7.0	9.4	5.2	7.3	12.1	6.4	7.9	12.0	6.8	9.1
50	54	11.4	6.2	7.6	10.1	5.8	7.3	8.9	5.1	7.6	11.8	6.1	8.1	14.9	7.5	10.7
150	41	11.6	6.1	7.8	10.8	5.8	7.6	9.4	4.9	7.6	11.6	6.2	8.6	18.8	8.5	12.2
250	28	12.0	5.6	7.9	11.4	5.5	7.7	9.6	4.8	7.9	11.3	5.6	8.9	19.7	8.8	13.3
350	15	12.3	5.6	8.0	11.6	5.6	7.9	10.0	4.6	8.2	11.5	5.4	8.9	20.1	7.9	13.8
512	15	12.6	5.6	8.0	12.2	5.5	8.3	9.9	4.6	8.6	12.1	5.1	9.0	21.6	8.4	14.2
675	15	13.2	6.3	8.5	13.1	3.1	8.3	9.8	4.7	8.1	11.3	5.1	8.7	21.3	8.1	14.8
838	15	13.8	6.4	8.7	13.2	6.1	8.5	10.3	4.9	8.1	10.6	5.1	8.8	19.7	8.4	13.8
1000	15	14.7	6.8	9.4	13.8	6.5	8.8	11.8	5.3	8.6	10.6	4.7	8.4	20.6	8.2	13.7
1100	28	15.1	7.0	9.3	13.9	6.6	9.0	11.2	5.7	9.1	10.2	4.8	8.1	22.3	9.5	15.1
1200	41	15.6	7.7	9.5	14.1	6.8	8.7	11.0	6.5	10.3	9.9	5.2	8.5	15.0	8.0	10.8
1300	54	16.4	8.0	9.6	14.5	7.2	8.8	11.5	7.0	10.6	9.6	5.4	8.1	17.2	8.3	11.3
1400	68	16.7	8.1	9.9	14.7	7.2	8.7	11.9	7.0	10.6	9.5	5.2	7.7	14.6	7.7	11.1
1500	81	16.8	8.5	9.5	13.5	6.6	8.1	12.3	7.0	10.8	10.1	5.4	7.6	12.7	7.3	11.3
1600	94	15.6	7.3	8.7	12.1	6.2	7.5	11.4	6.7	10.0	11.0	5.6	7.6	10.6	6.3	9.6
1700	107	11.9	6.8	8.1	10.3	5.2	6.4	10.2	5.8	8.6	12.2	6.0	7.9	9.2	5.0	6.8
1875	130	11.0	5.8	6.7	9.0	4.7	6.3	9.2	5.1	7.3	10.0	6.0	8.7	7.9	4.6	6.5
2050	153	7.6	4.6	5.3	6.6	3.8	4.9	6.3	4.1	5.5	5.7	3.6	5.5	6.3	4.3	5.8
2200	174	6.0	3.7	4.7	5.4	3.7	4.4	4.3	2.9	4.4	5.0	3.6	4.8	5.4	4.0	5.0
2350	194	4.2	2.9	3.1	5.0	3.6	4.1	4.5	3.2	4.6	4.9	3.5	4.6	6.0	4.0	4.8
2650	233	4.9	3.3	3.9	5.2	3.9	4.3	4.6	3.3	4.4	5.0	3.4	4.0	5.1	3.7	4.7
2950	272													4.9	3.7	4.6
3550	350													3.2	3.0	3.1

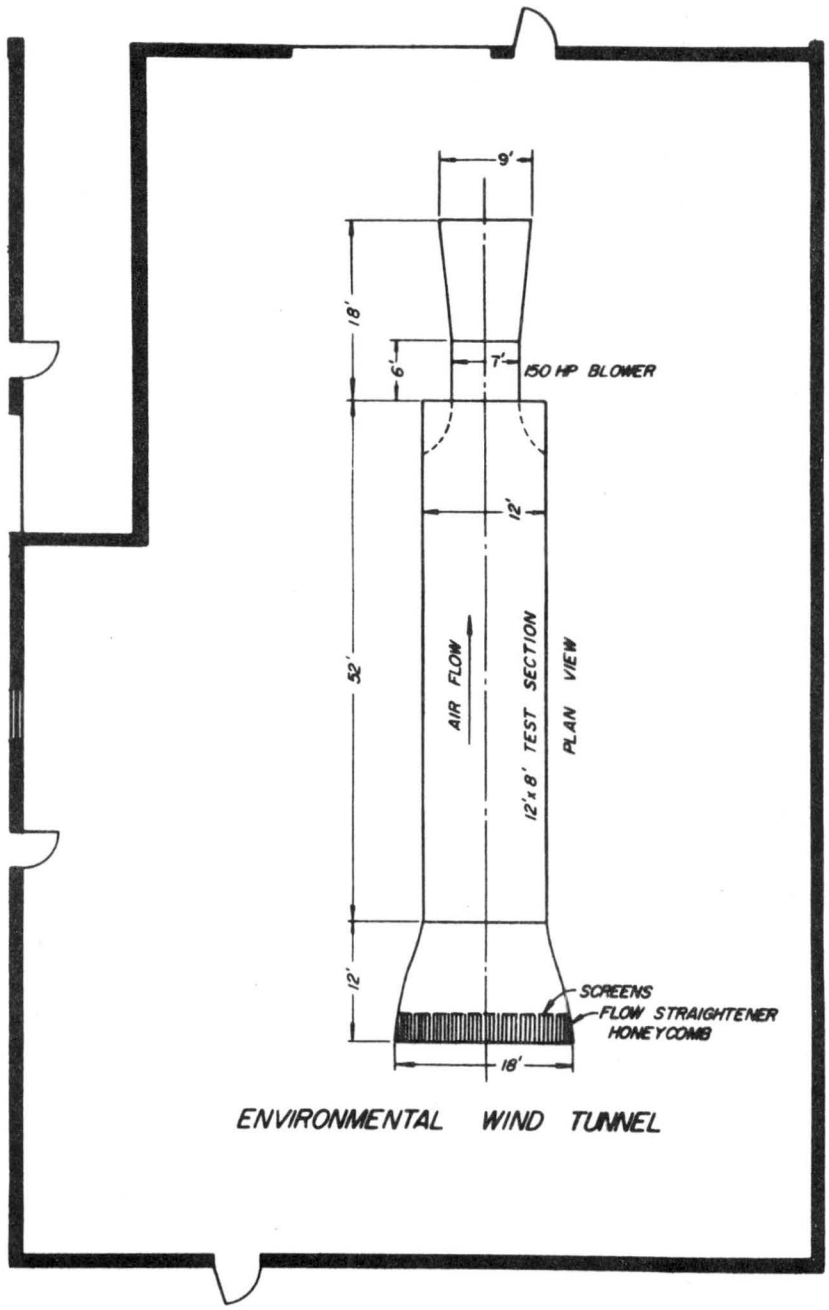

Figure 1. Plan View of Environmental Wind Tunnel

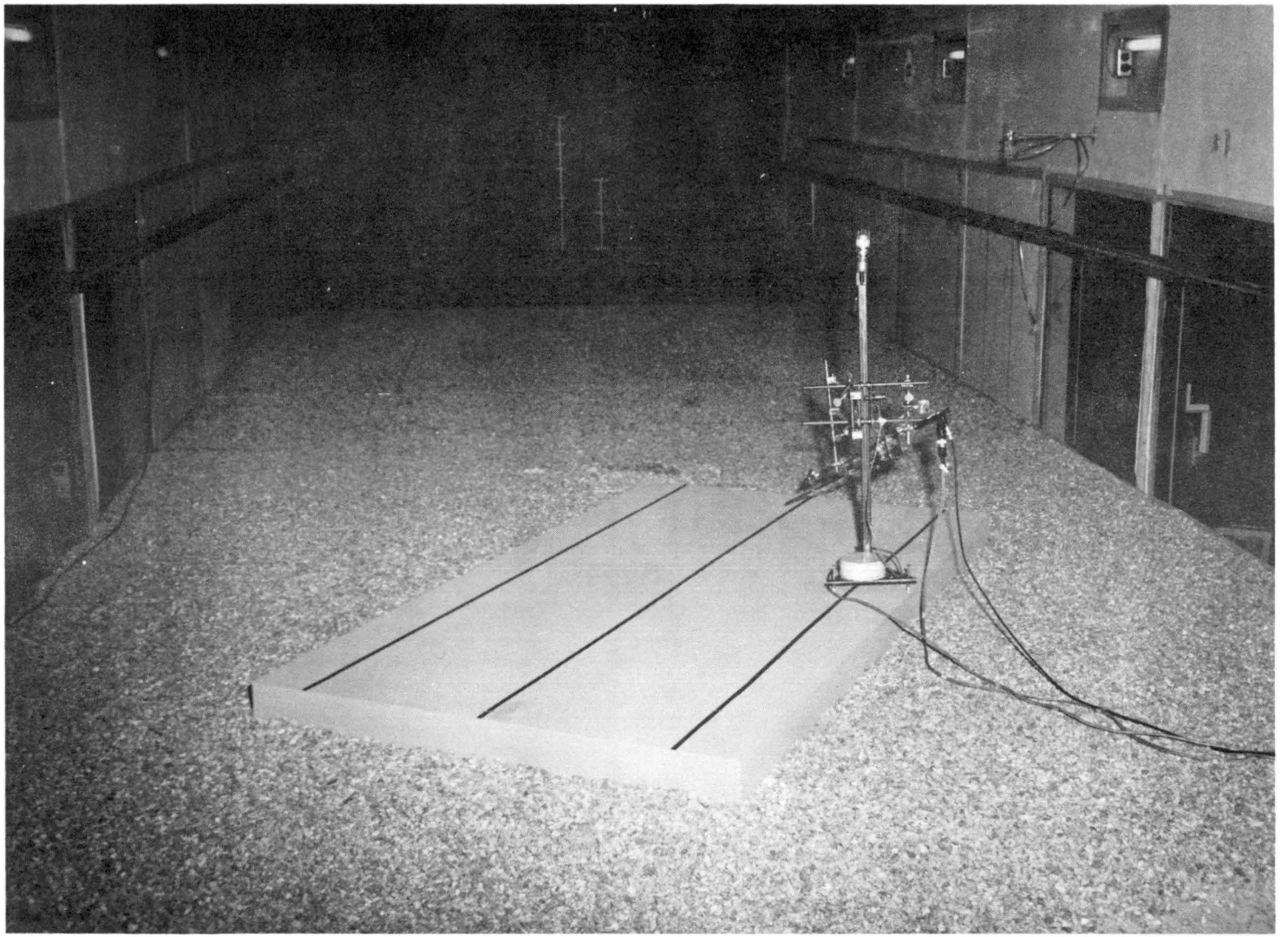

Figure 2. Model installed in the wind tunnel for 30 degree wind.

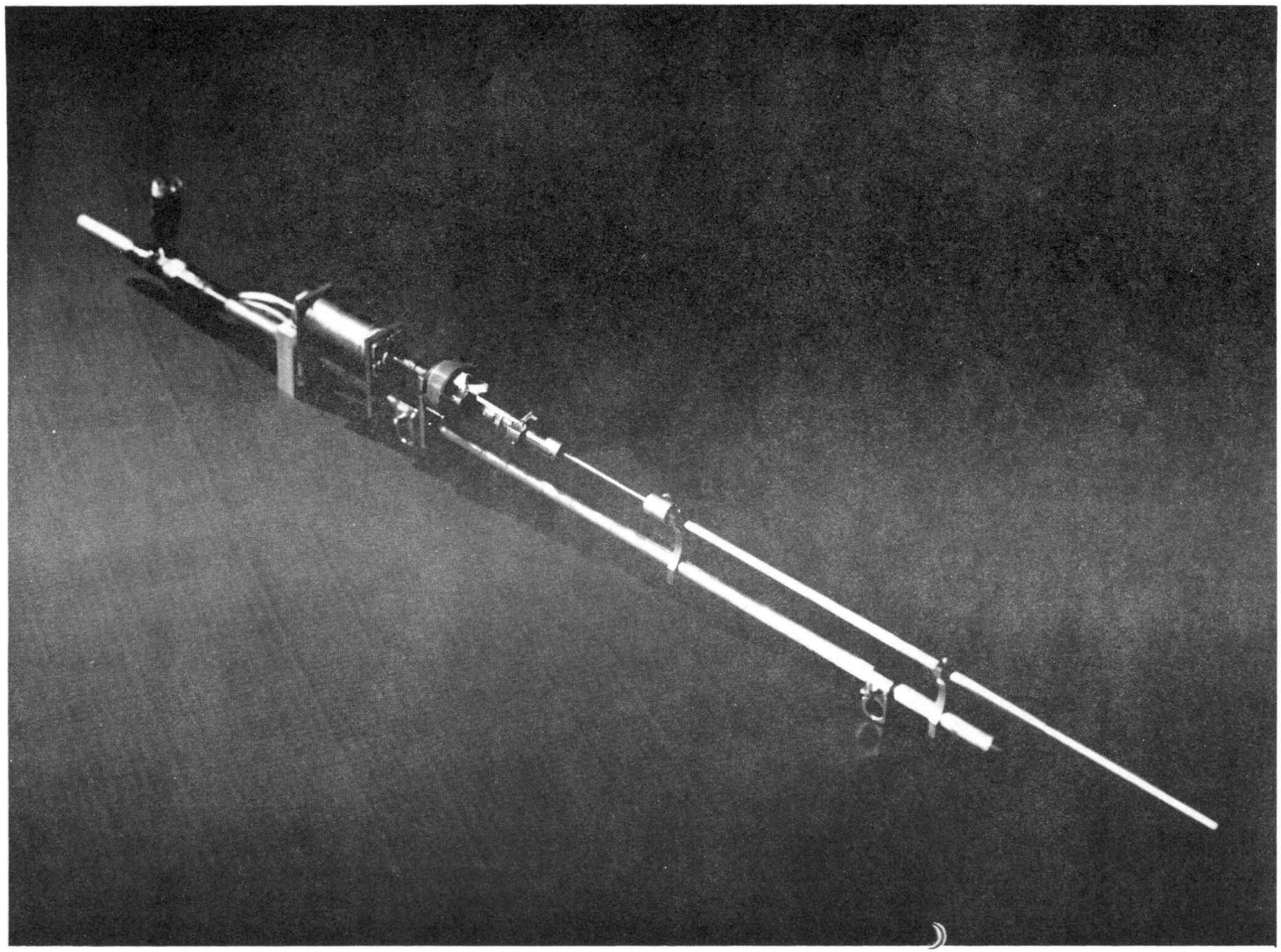

Figure 3. Hot Wire probe.

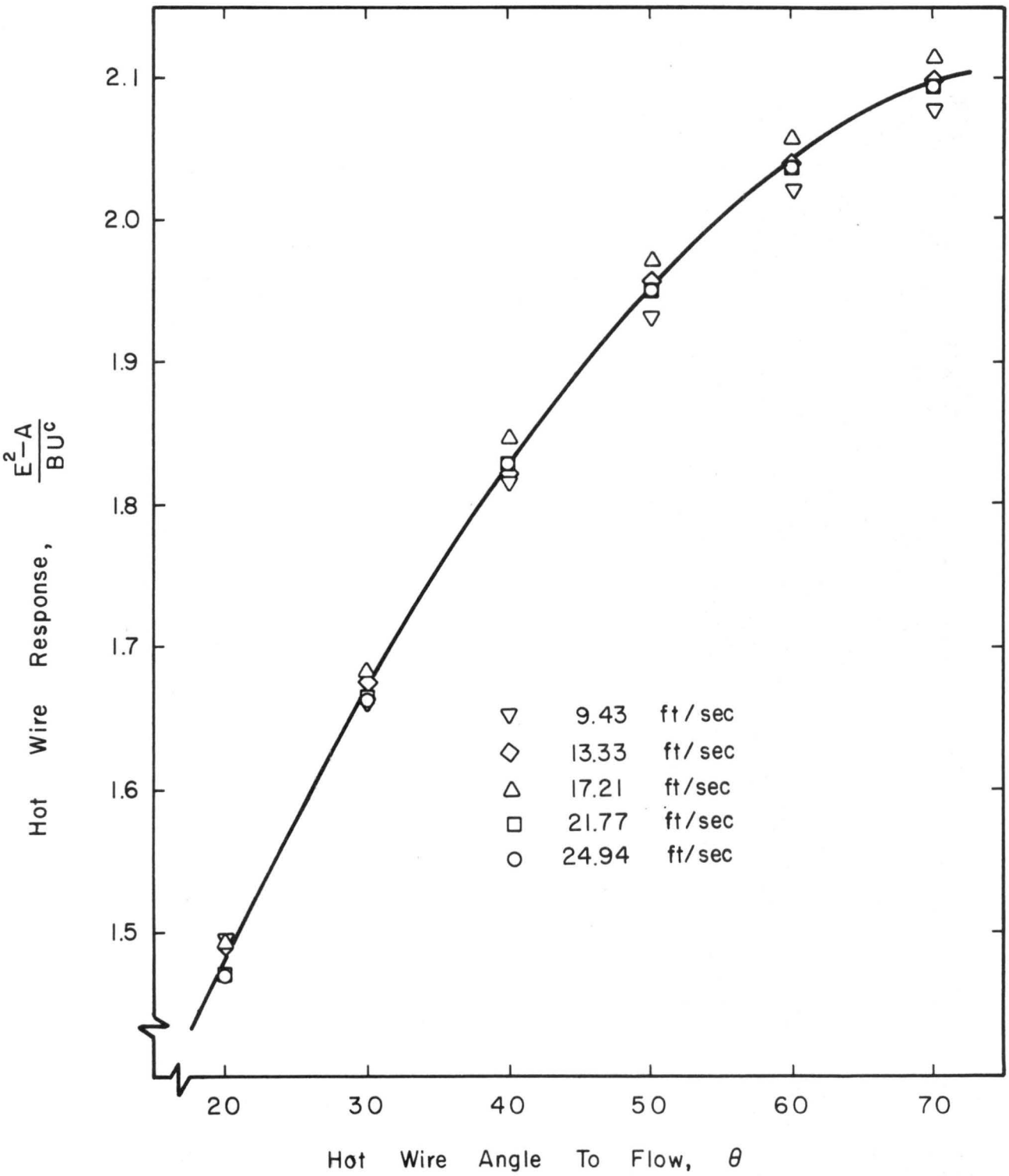

Figure 4. Typical hot-wire calibration

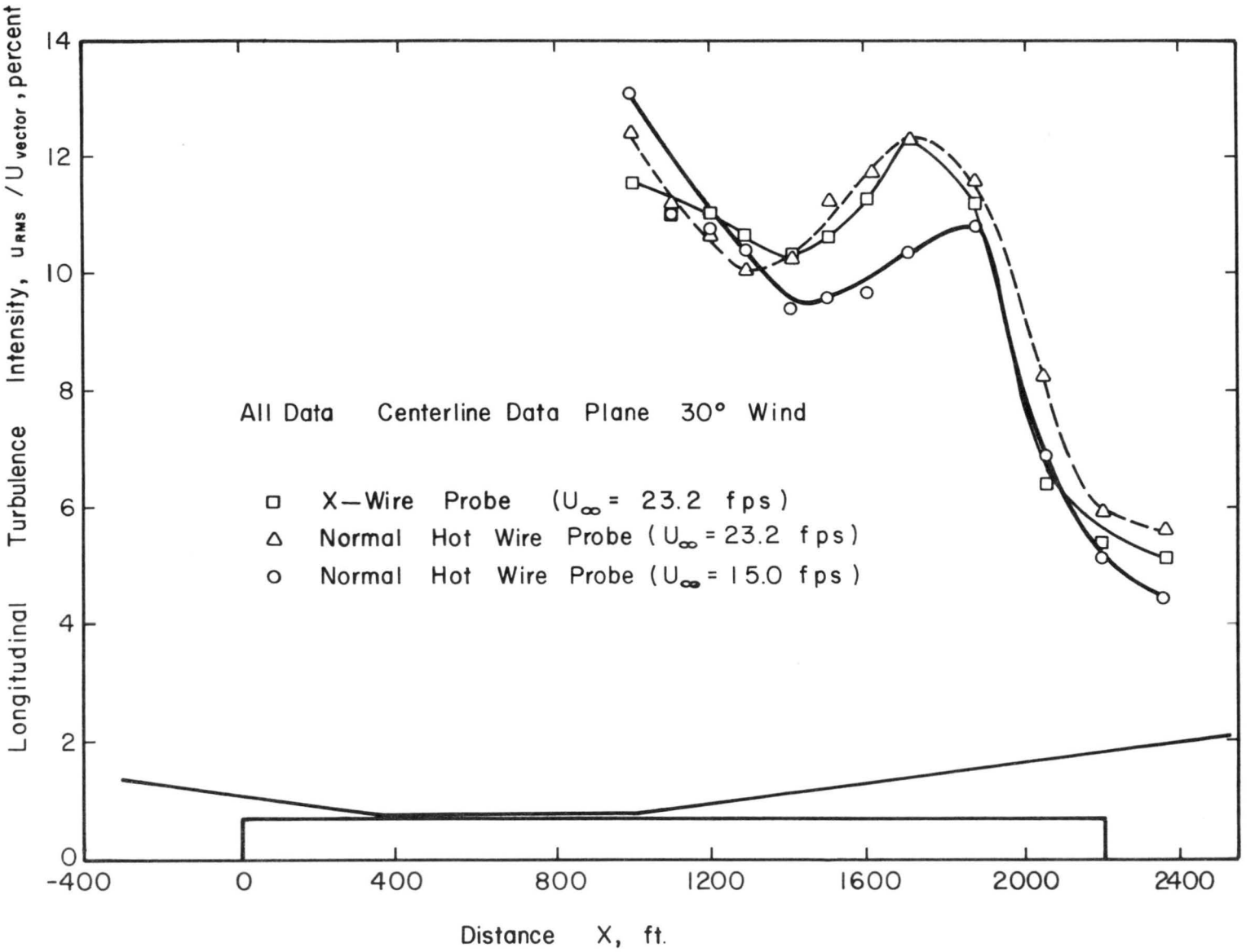

Figure 5. Results of hot-wire anemometer turbulence validation tests

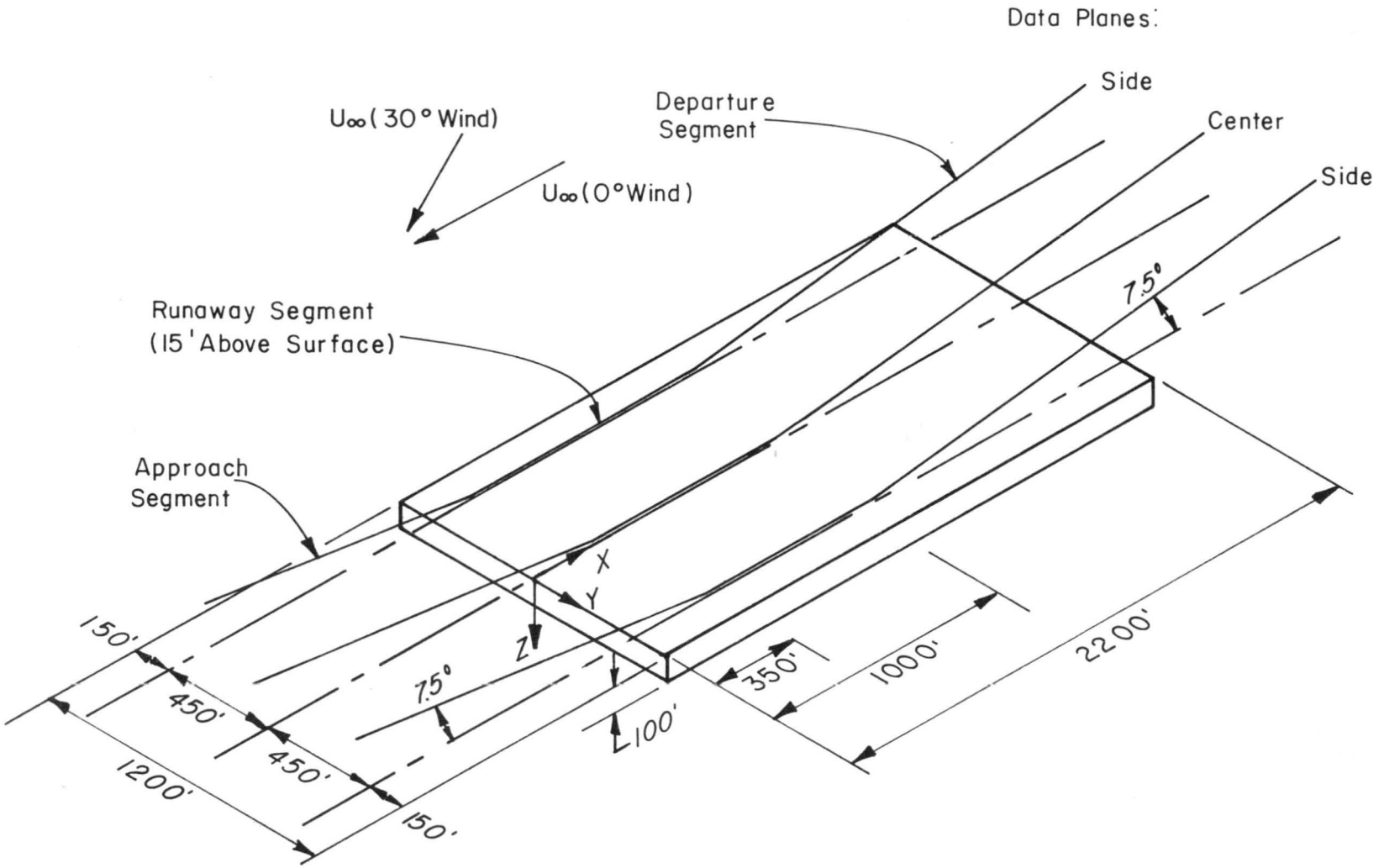

Figure 6. Data lines and coordinate system

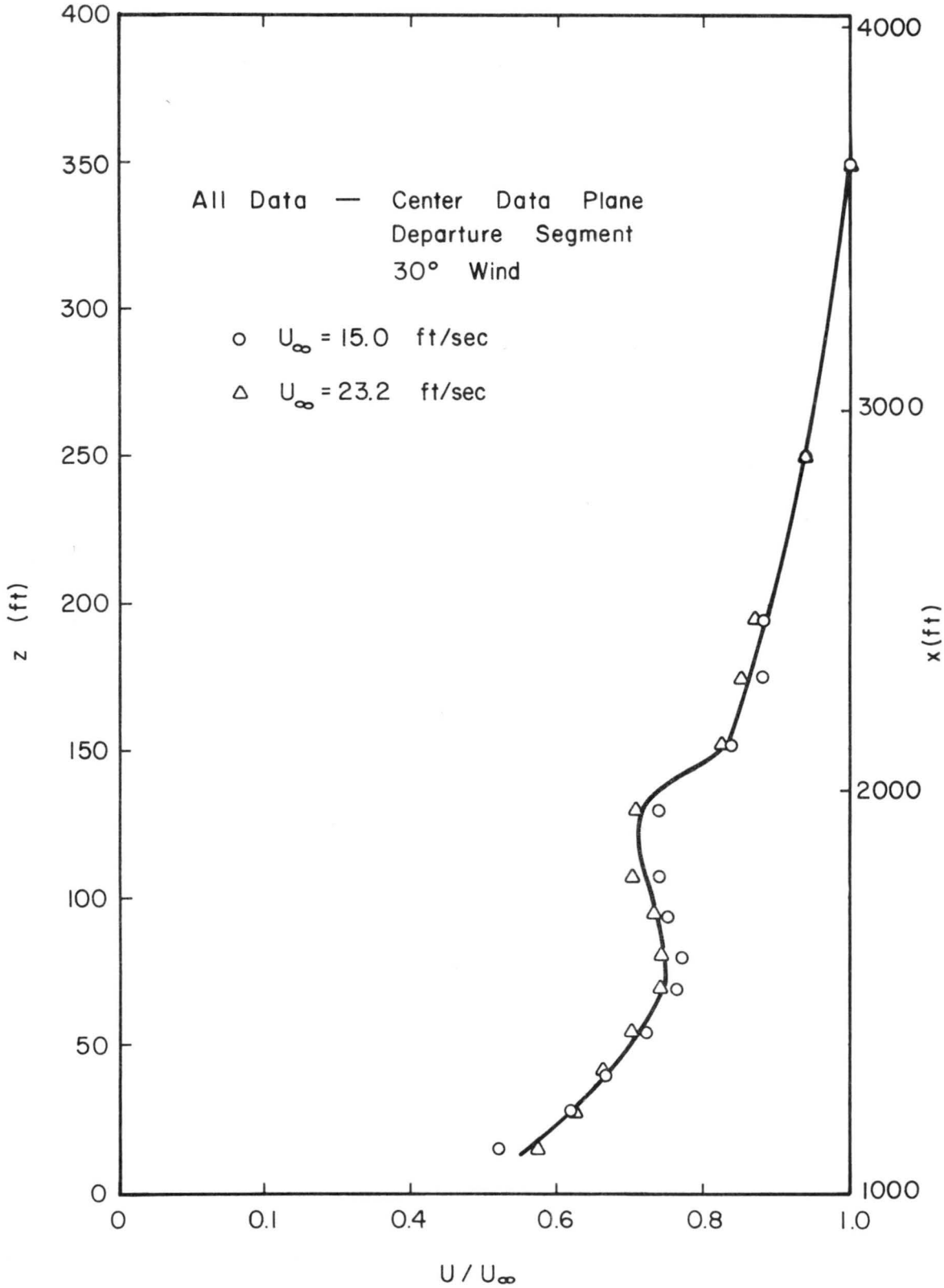

Figure 7. Demonstration of Reynolds number independence for velocity

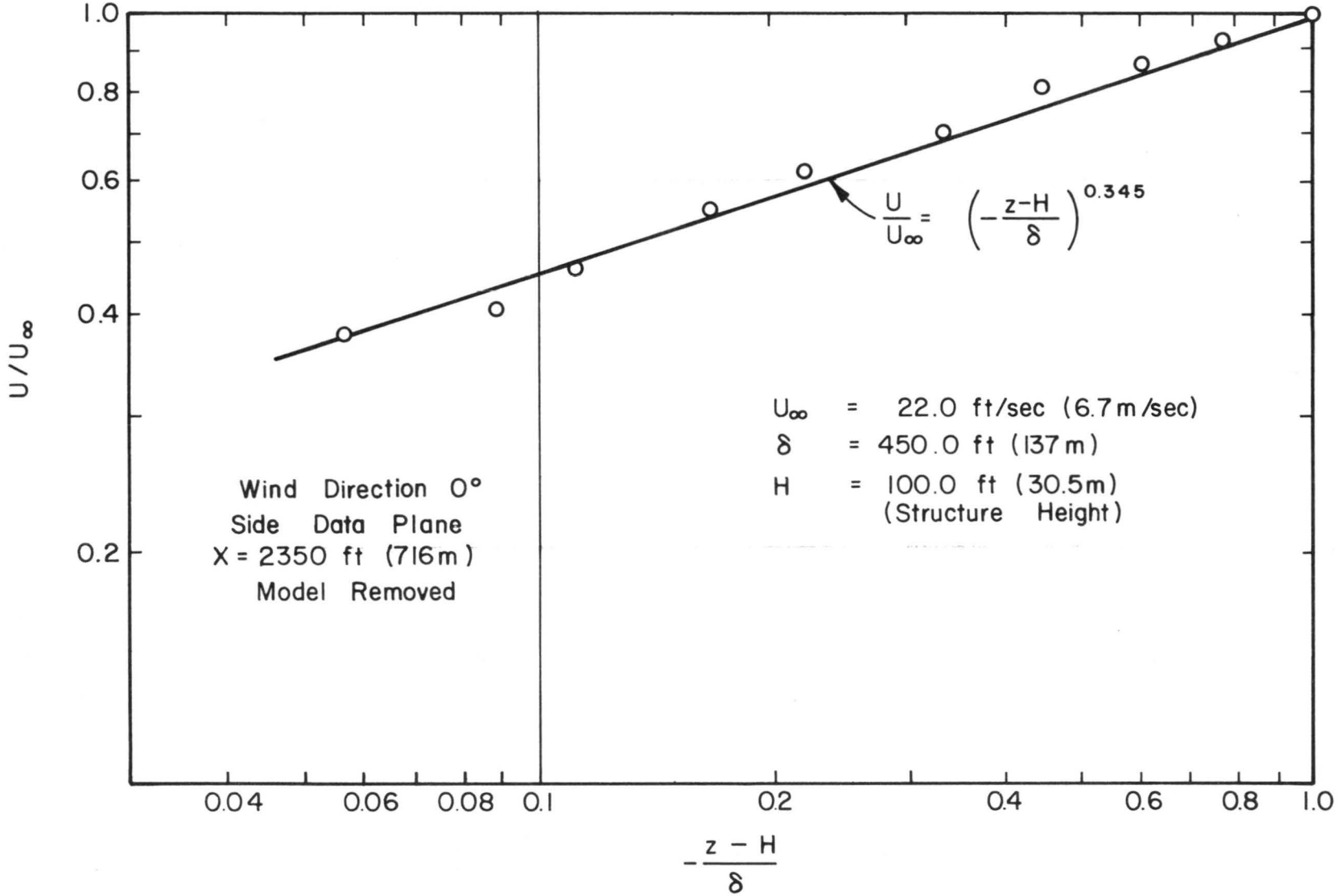

Figure 8. Mean velocity profile in logarithmic form

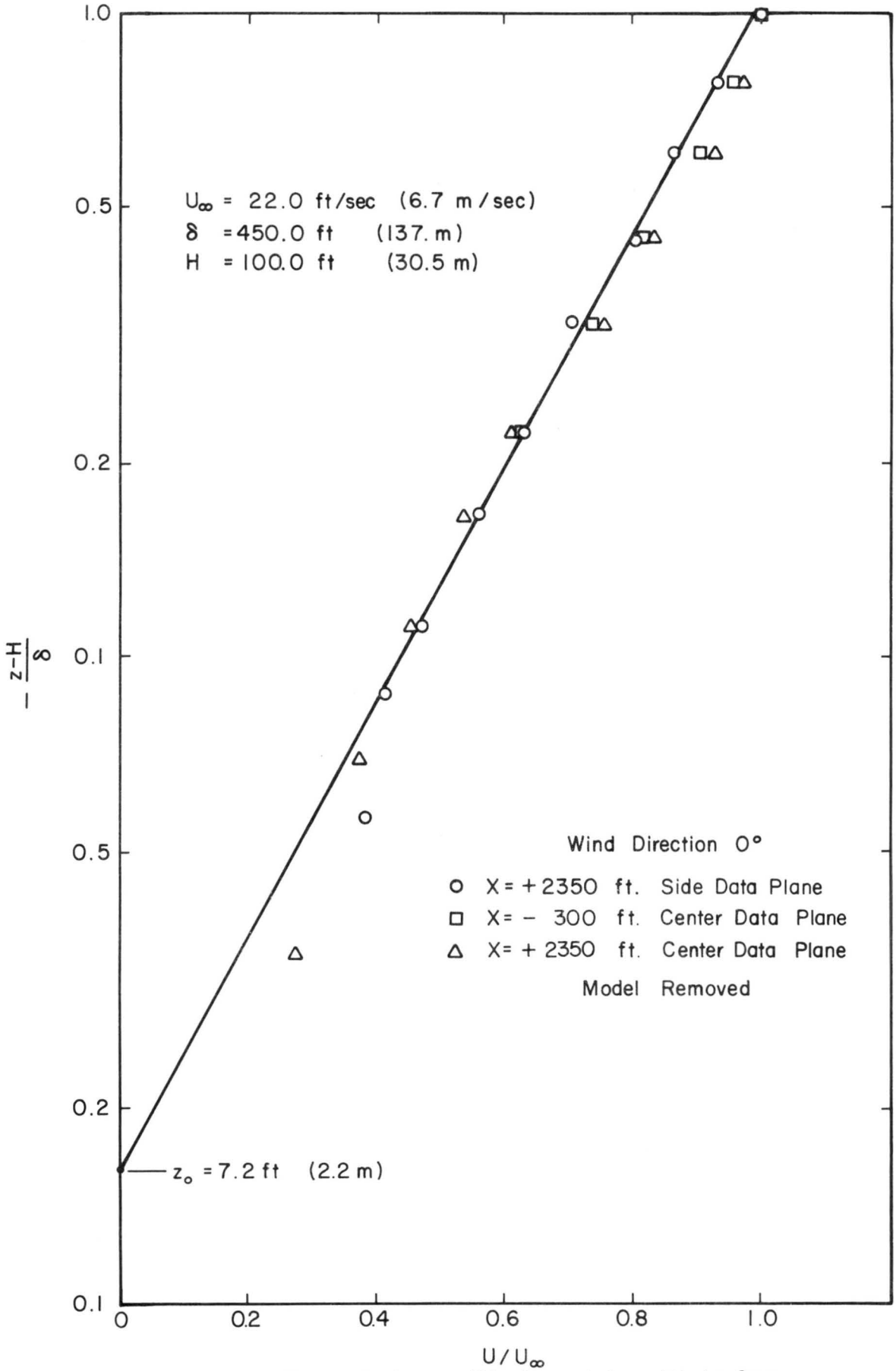

Figure 9. Mean velocity profile in semi-logarithmic form

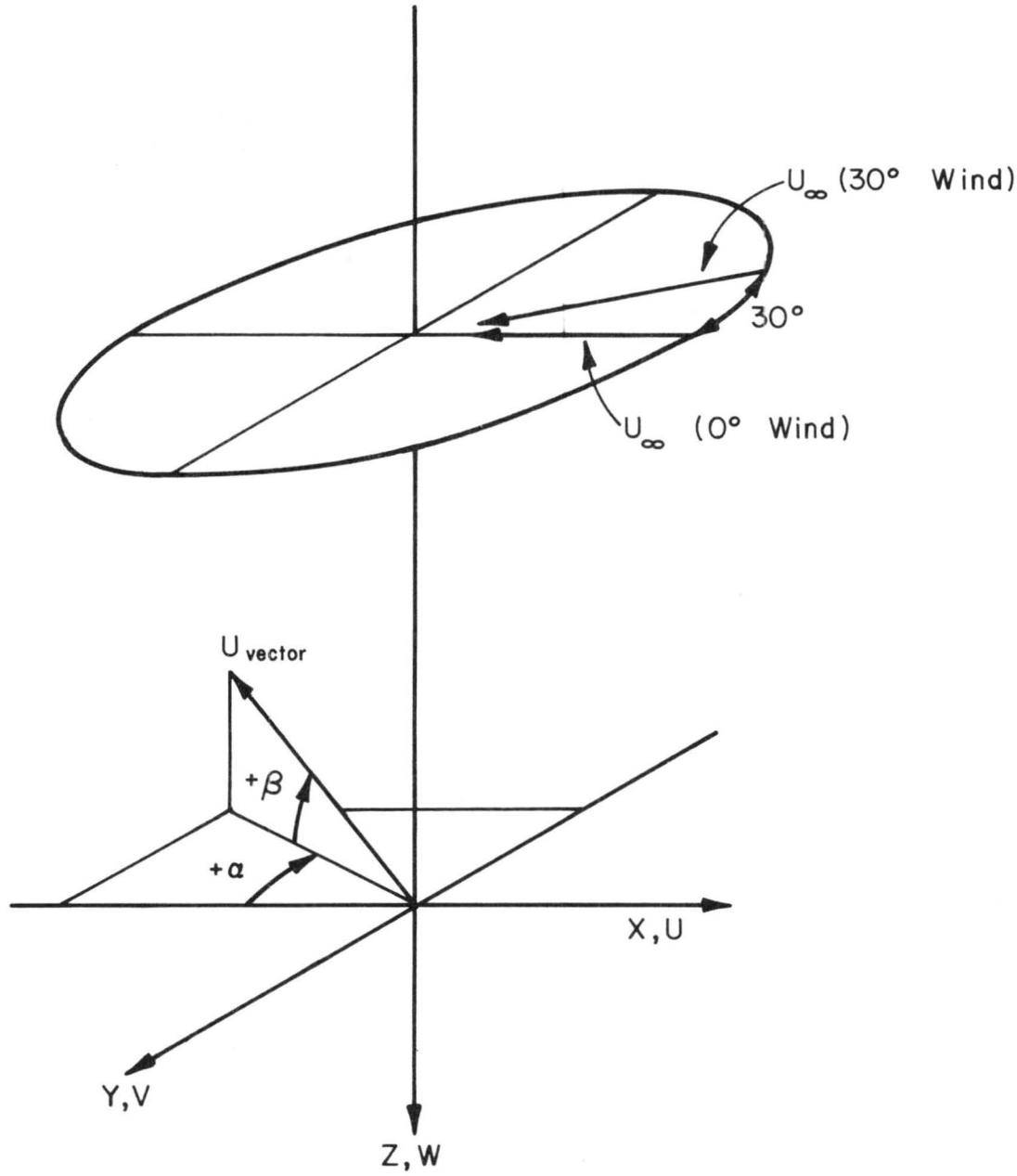

Figure 10. Definitions of angles α and β

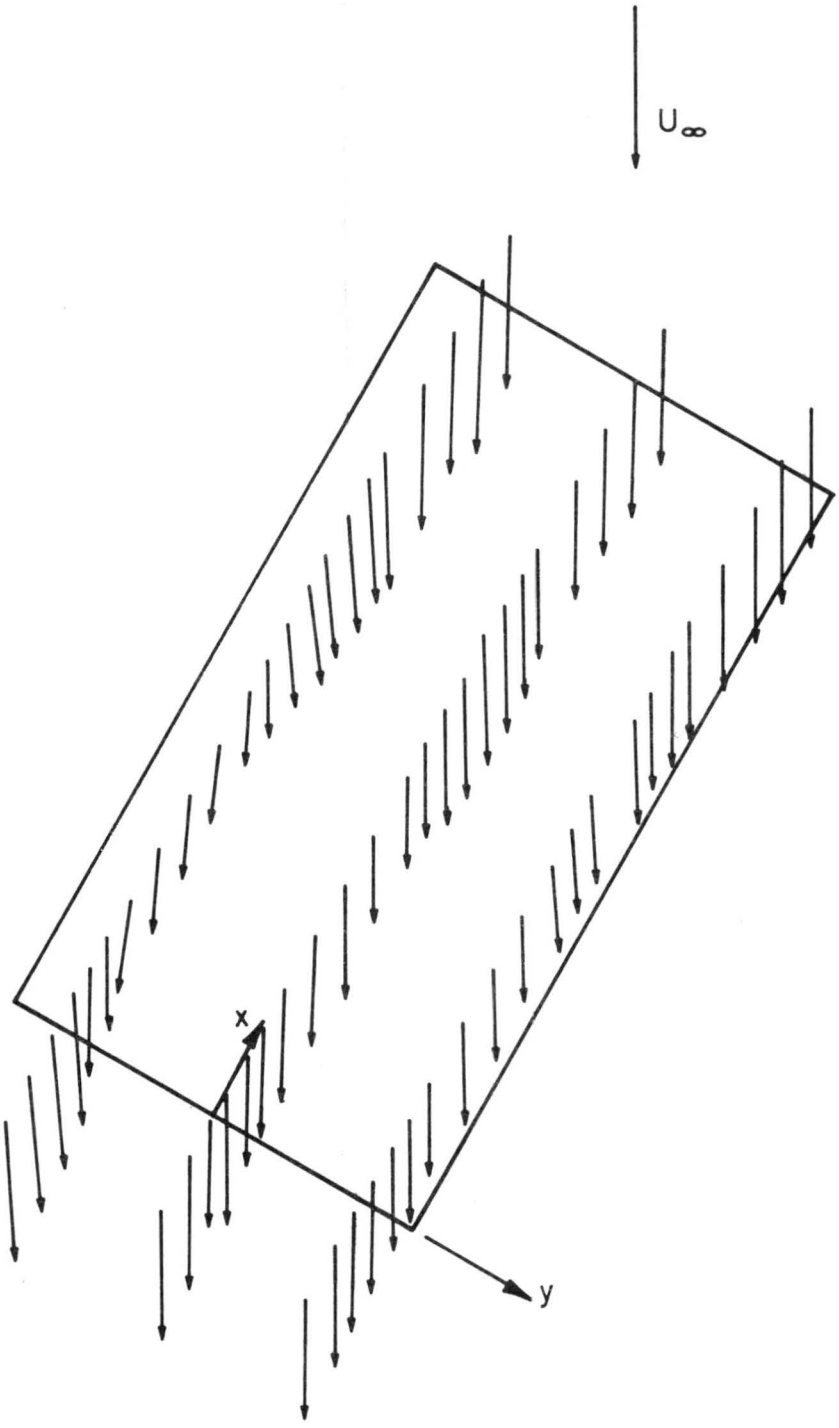

Figure 11. Mean flow magnitude and direction for 30 degree wind

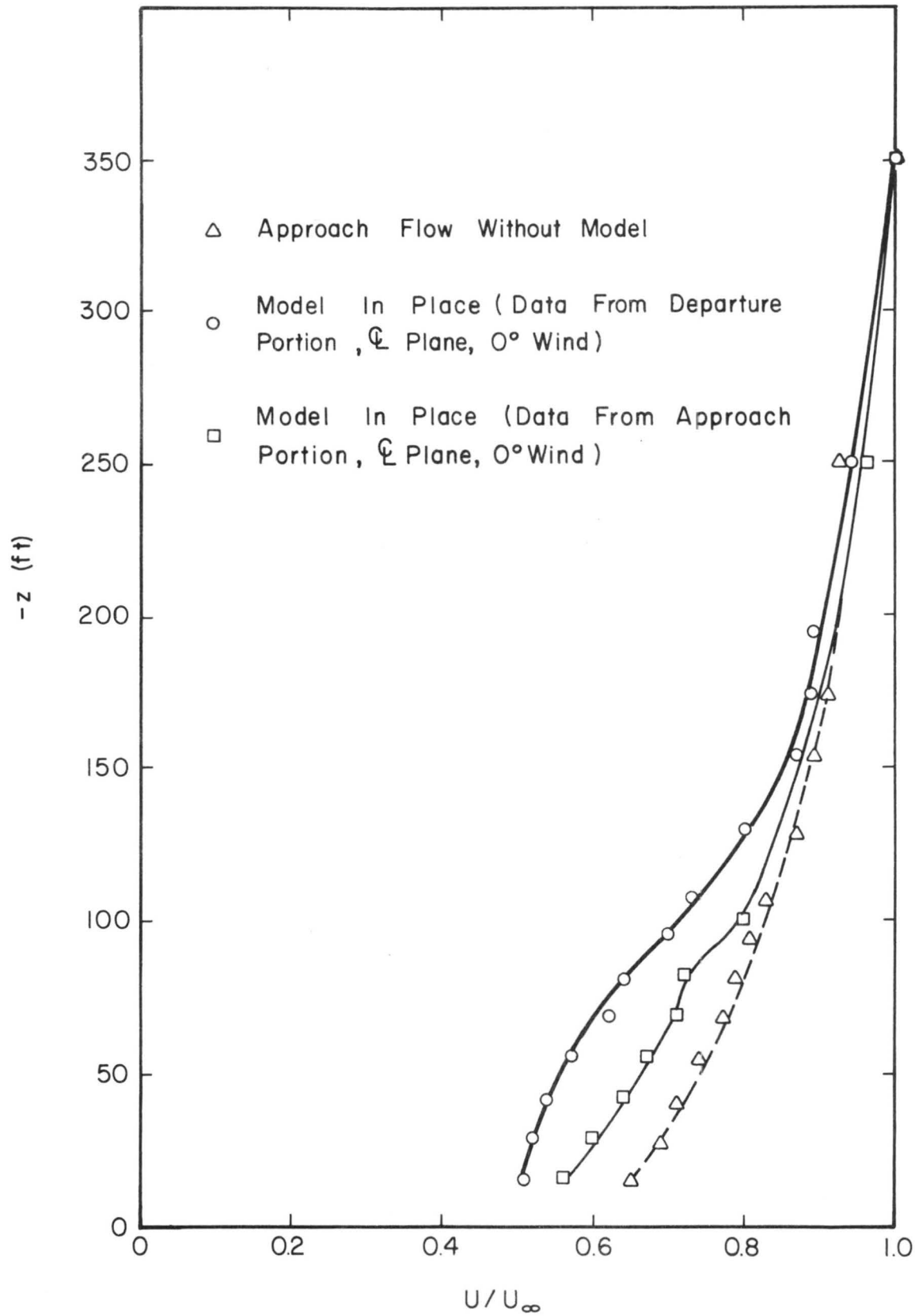

Figure 12. Mean velocity with and without model in place

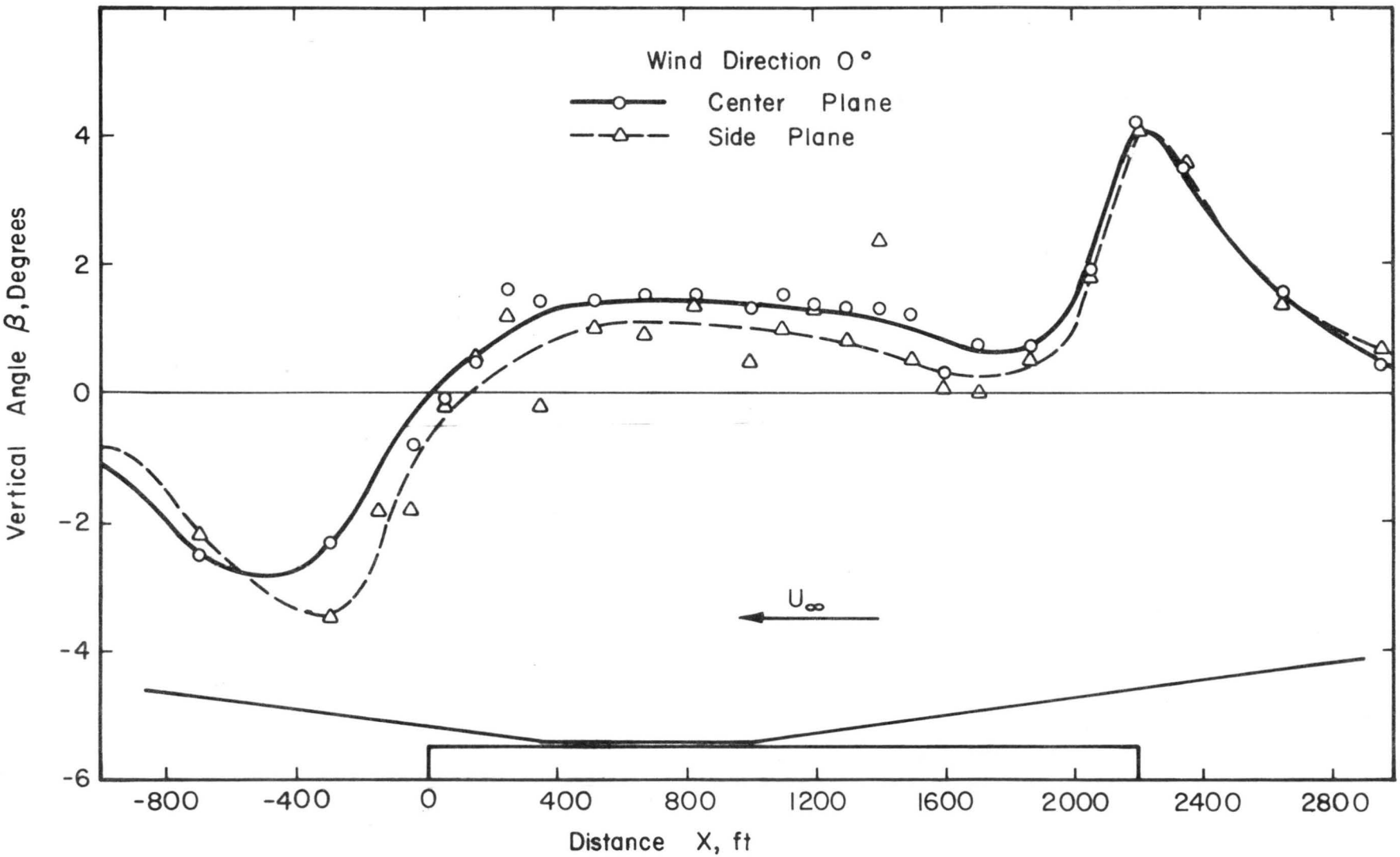

Figure 13. Vertical flow angles for 0 degree wind

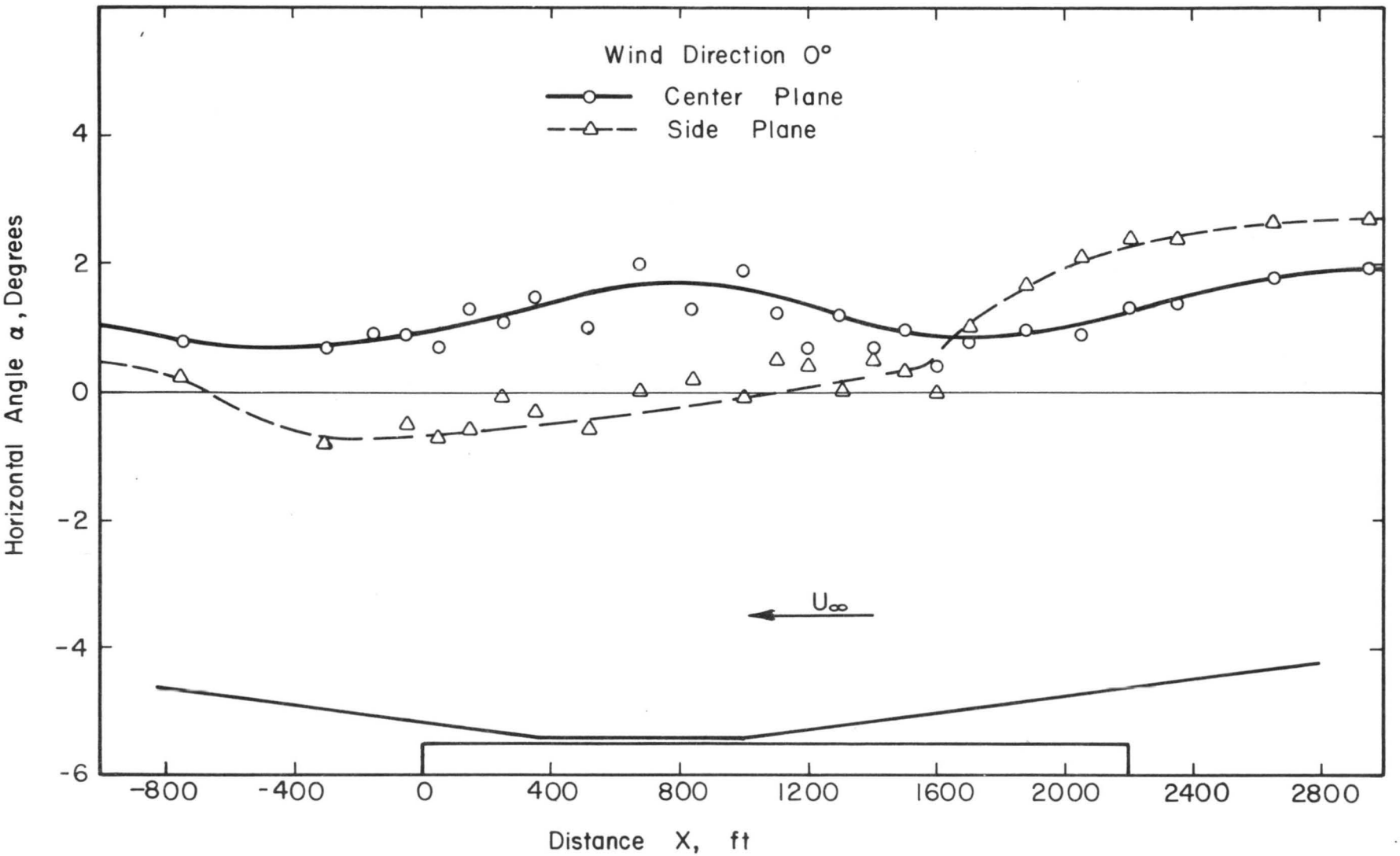

Figure 14. Horizontal flow angles for 0 degree wind

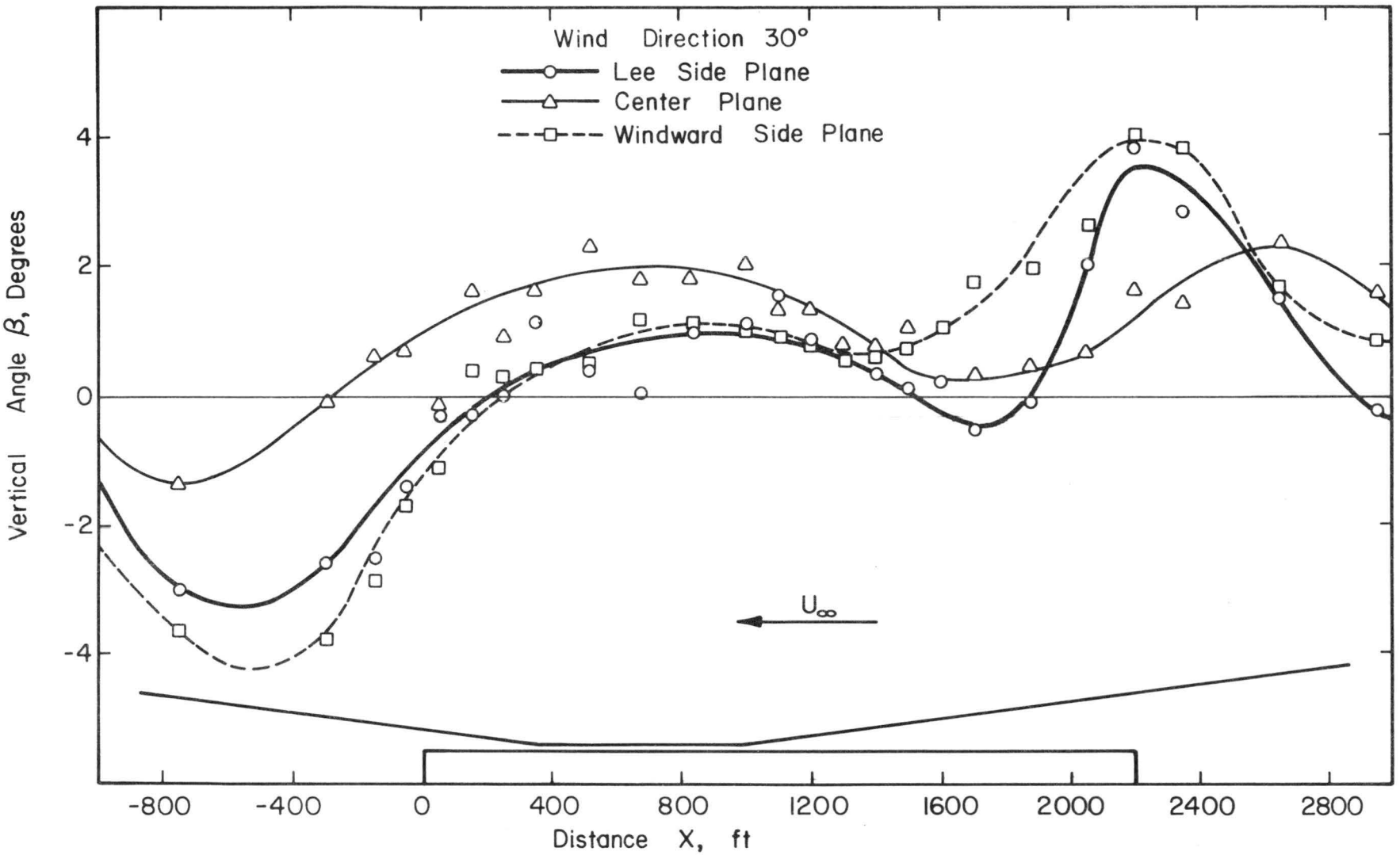

Figure 15. Vertical flow angles for 30 degree wind

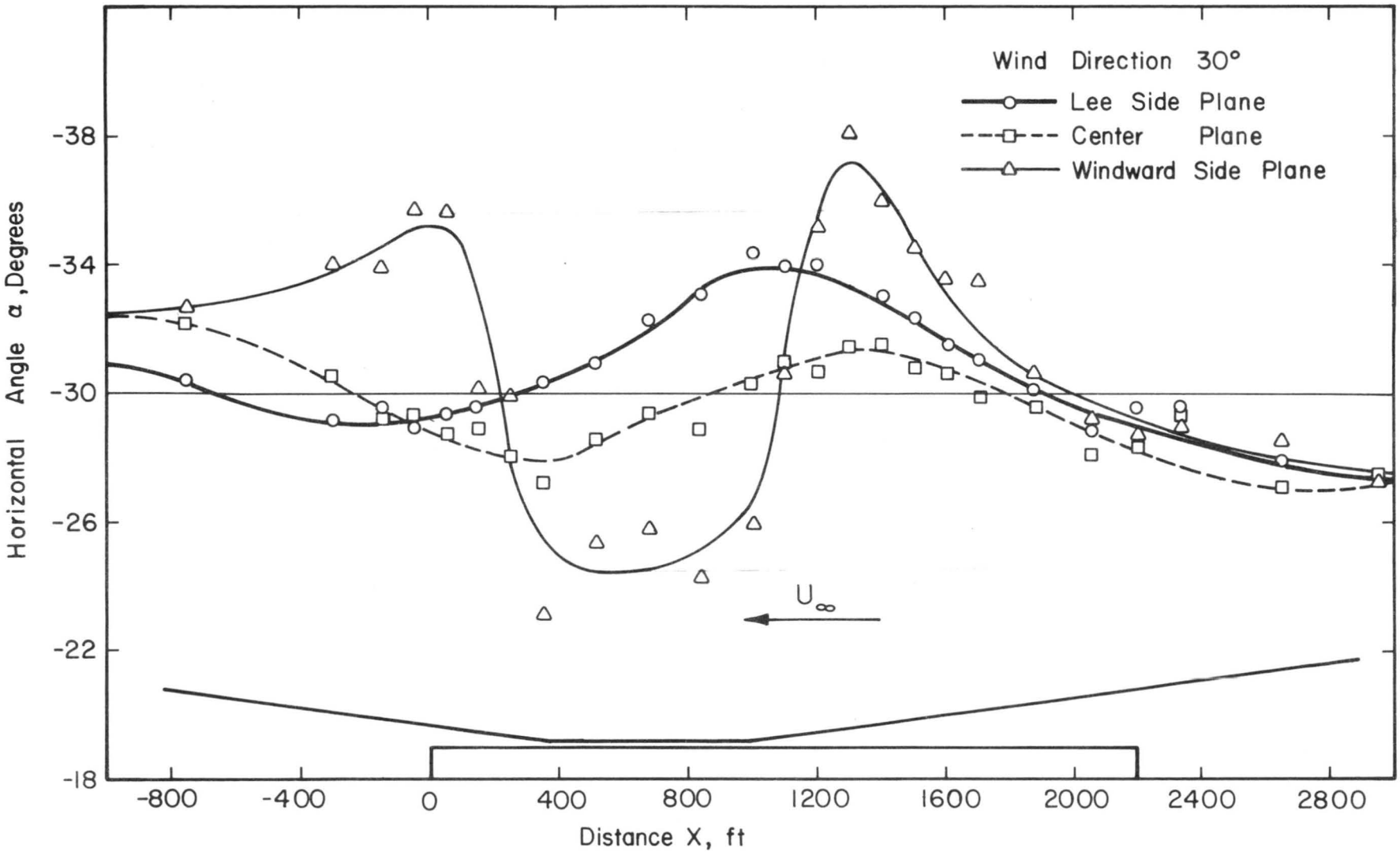

Figure 16. Horizontal flow angles for 30 degree wind

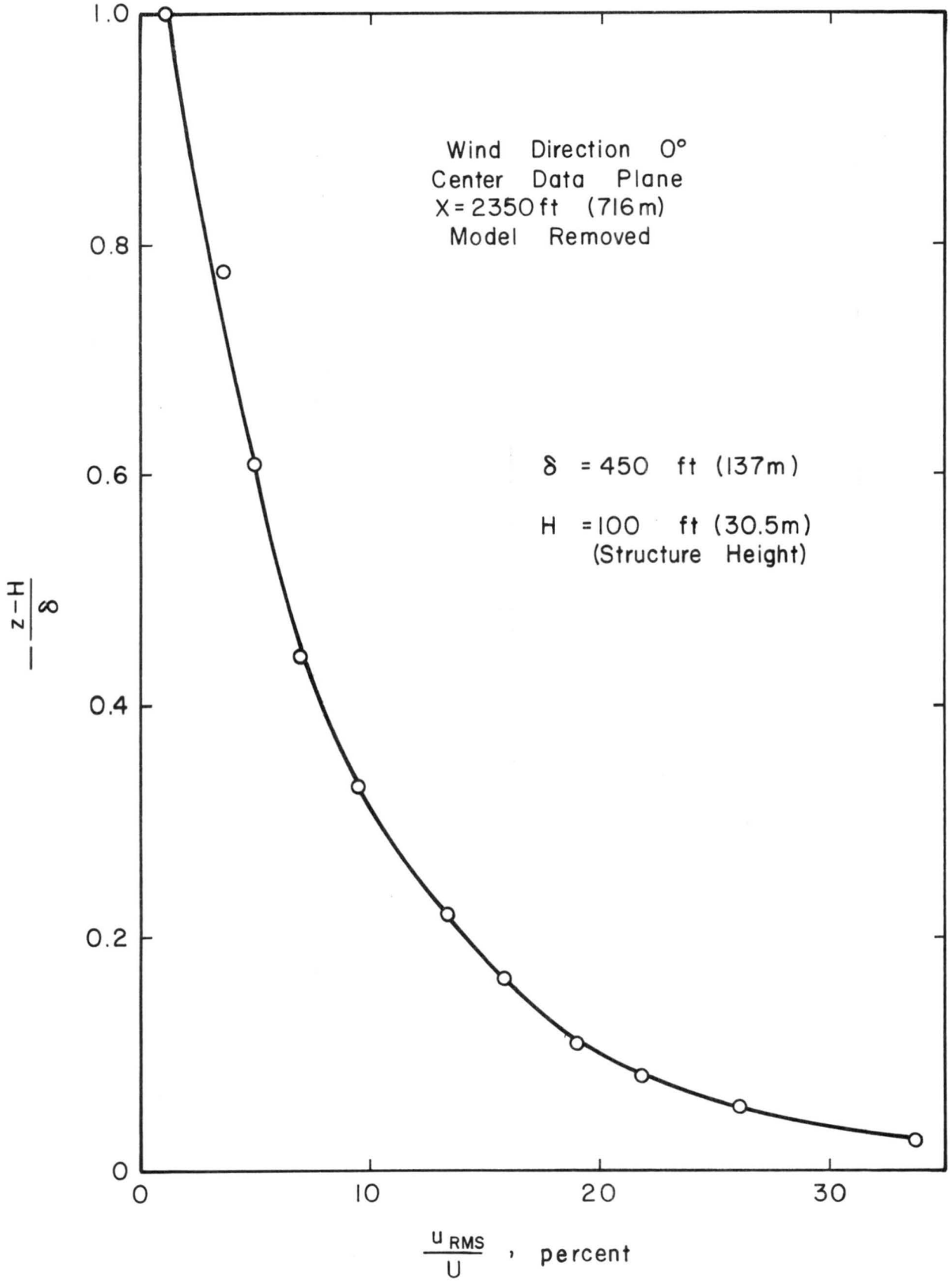

Figure 17. Longitudinal turbulence intensity without model

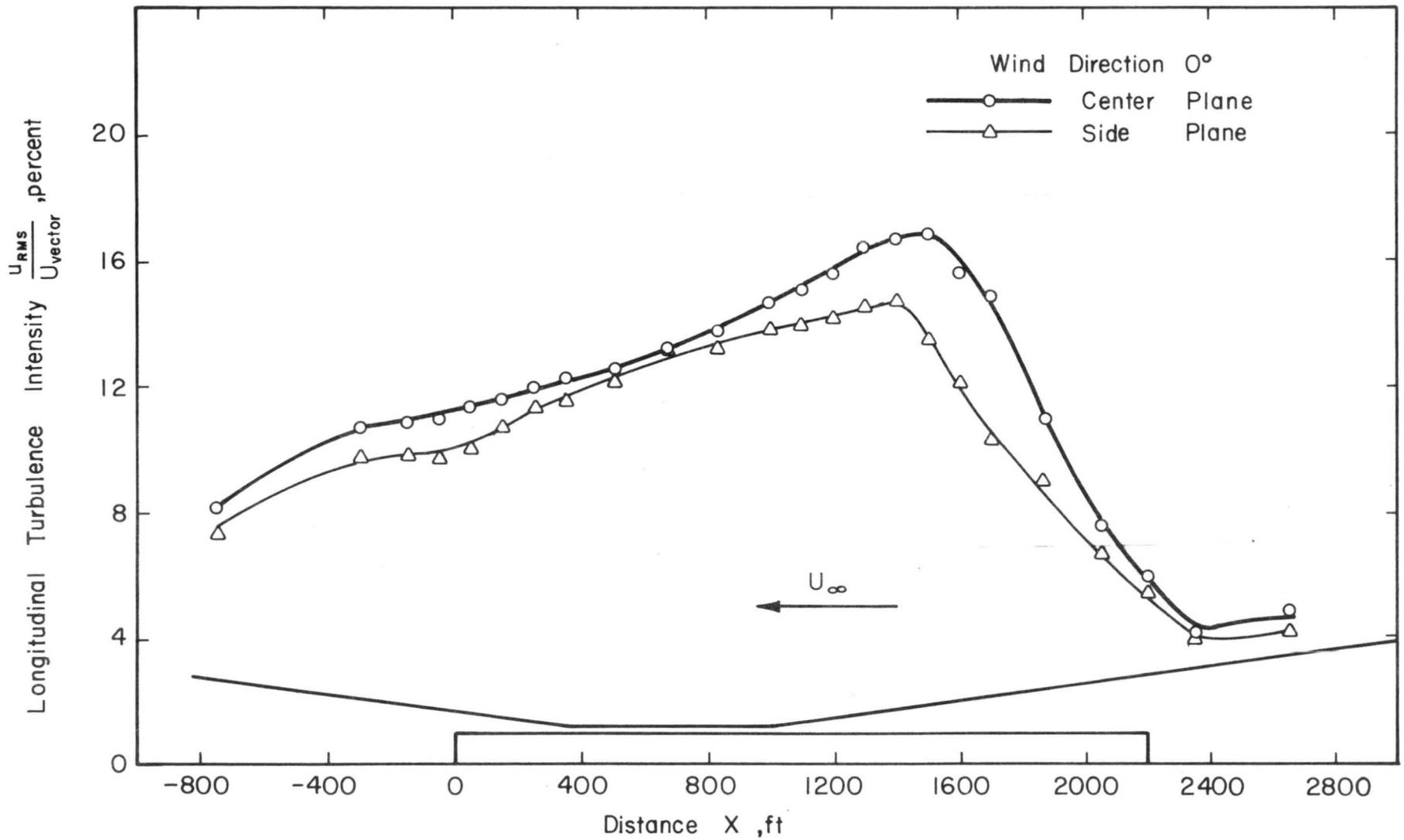

Figure 18. Longitudinal turbulence intensity for 0 degree wind

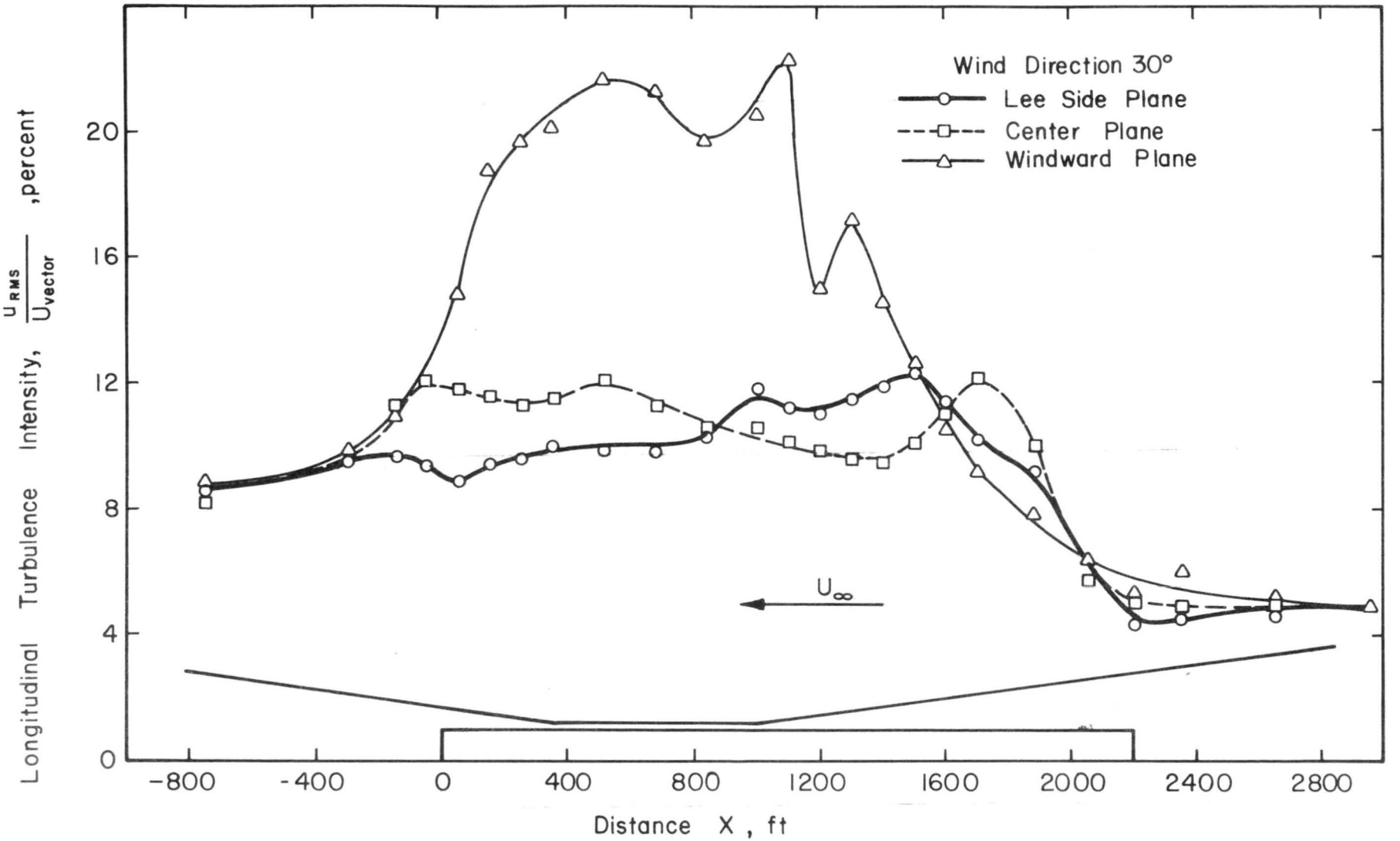

Figure 19. Longitudinal turbulence intensity for 30 degree wind